STATISTICAL RELATION OF TRAVELING IONOSPHERIC DISTURBANCES WITH NEUTRAL WIND AND DISTURBANCES IN THE STRATOSPHERE

M.V. Tolstikov
Institute of Solar-Terrestrial Physics SB RAS,
Irkutsk, Russia, maxim@iszf.irk.ru

A.V. Oinats
Institute of Solar-Terrestrial Physics SB RAS,
Irkutsk, Russia, oinats@iszf.irk.ru

M.F. Artamonov
Institute of Solar-Terrestrial Physics SB RAS,
Irkutsk, Russia, artamonov.maksim@iszf.irk.ru

I.V. Medvedeva
Institute of Solar-Terrestrial Physics SB RAS,
Irkutsk, Russia, ivmed@iszf.irk.ru

K.G. Ratovsky
Institute of Solar-Terrestrial Physics SB RAS,
Irkutsk, Russia, ratovsky@iszf.irk.ru

Abstract. Using the representative statistics on traveling ionospheric disturbances (TIDs) obtained by Yekaterinburg and Magadan radars, we have shown that distributions of TIDs and average TID velocities by azimuths and local time agree well with the hypothesis on internal gravity wave (IGW) filtering by the neutral wind. We have examined the influence of significant winter sudden stratospheric warmings on IGW in the ionosphere. A method has been proposed for estimating zonal and meridional neutral wind velocities from MSTID parameters. The method is universal and allows us to estimate the zonal and meridional neutral wind velocities from the statistics on MSTID 2D phase velocity vector obtained by any tool. There is a large amount of data from which MSTID 2D phase velocity vector (as opposed to the 3D phase velocity vector) can be derived, including maps of TEC disturbances and all-sky camera images. This method may therefore be useful in developing and improving neutral wind models.

Keywords: TIDs, MSTIDs, IGWs, hypothesis on IGW filtering by the neutral wind, neutral wind, sudden stratospheric warmings.

INTRODUCTION

Internal gravity waves (IGWs) make a significant contribution to the general circulation of the atmosphere, the formation of its global structure and dynamics [Fritts, Alexander, 2003; Alexander et al., 2008]. Ionospheric effects of IGWs are traveling ionospheric disturbances (TIDs). It is these disturbances that are used for experimentally investigating IGWs in the thermosphere. Various ionospheric plasma instabilities [Otsuka, 2021; Shiokawa et al., 2003, 2009; Ivanov, Tolsytikov, 2003] can, however, also be a source of TIDs, which complicates the analysis of IGWs from ionospheric data. One of the ways to separate TIDs into those driven by IGWs and those of a different physical nature is to check the measured parameters for correspondence with the dispersion equation, which relates the wave vector and IGW frequency to the known parameters of propagation medium [Pedlosky, 2003, Hines, 1960]. This method works when the TID full 3D phase velocity vector is measured, which, in turn, requires measuring the vertical electron density profiles at minimum three spaced points. Such measurements have been carried out with multipath incoherent scatter radars and complexes of several radiophysical instruments [Ma et al., 1998; Nicolls, Heinselman, 2007; Vadas, Nicolls, 2008; Nicolls et al., 2014; Van de Kamp et al., 2014; Vlasov et al., 2011]. In [Williams et al., 1982], the Hines dispersion equation was first tested for a single measurement. The study showed a good fit of the Hines equation to ~40 min TIDs, but at the same time posed a problem of considering the neutral wind. Vadas and Nicolls [2008] have proposed a method of determining the neutral wind velocity projection on the TID propagation direction under the assumption that the dispersion equation is satisfied. Medvedev et al. [2015, 2017, 2019] have tested the Hines dispersion equation, using the representative statistics on measurements of the TID full velocity vector. These works have shown that most experimental data correlates well with the theoretical ideas about IGW propagation in the upper atmosphere, and have proposed a method of obtaining meridional and zonal neutral winds from the statistics on measurements of the TID full velocity vector. Neutral wind parameters are in good agreement both with the HWM07-14 model data [Drob et al., 2008, 2015] and with independent autocorrelation measurements of the Irkutsk Incoherent Scatter Radar [Shcherbakov et al., 2015].

The key concept we apply in this paper is the hypothesis on IGW filtering by the neutral wind (wind-filtering hypothesis). As an empirical fact, wind filtering implies that most TIDs occur when their propagation direction is close to the direction opposite to the velocity of the background wind [Kalikhman, 1980; Waldock, Jones, 1984, 1986; Crowley et al., 1987]. From a theoretical perspective, the wind-filtering hypothesis suggests that IGW propagation downwind significantly

reduces the wave amplitude due to dissipation, whereas IGW propagation upwind increases the wave amplitude. This hypothesis has been confirmed by studies using numerical simulation [Pogoreltsev, Pertsev, 1996]. An important refinement to the wind-filtering hypothesis is the wind-filtering mechanism at a critical level [Negale et al., 2018]: IGWs propagating upwind have a longer vertical wavelength and are much less affected by molecular viscosity than IGWs propagating downwind and having a shorter vertical wavelength. In our previous studies, this hypothesis was tested using data from different instruments [Medvedev et al., 2017; Tolstikov et al., 2019, 2020] and the empirical neutral wind models HWM07 and HWM14 [Drob et al., 2008, 2015]. The testing has shown that the behavior of most TIDs accords with the wind-filtering hypothesis, and the exceptions can be explained by errors in the neutral wind models or by the cases when the observed disturbances were not associated with IGWs. It is not always possible to measure the TID full phase velocity vector. A lot of papers have been published which estimate only the TID 2D phase velocity vector, using data from different instruments [Afraimovich et al., 2000; Shiokawa et al., 2003, 2009; Huang et al., 2016; Yang et al., 2017; Lay et al., 2018; Syrenova et al., 2022]. In particular, Oinats et al. [2015, 2016a, b] used data from coherent HF radars, similar to those included in SuperDARN, to conduct a statistical study into medium-scale TIDs (MSTID) based on horizontal velocity vector measurements. With such measurements, it becomes impossible to directly test the dispersion equation. Nonetheless, to indirectly separate MSTIDs of different nature, we can use the wind-filtering effect, which is manifested only in IGW propagation.

In this paper, we statistically analyze the data from the Ekaterinburg radar for 2012–2021 and from the Magadan radar for 2021. We delve into the influence of major stratospheric warmings on MSTIDs in the ionosphere and propose a method for estimating zonal and meridional neutral wind velocities from distributions of MSTID 2D parameters. The method is universal and can estimate the zonal and meridional neutral wind velocities

from the statistics on observations of the two-dimensional phase velocity vector of MSTIDs obtained by any instrument. There is a large amount of data from which we can determine the IGW 2D phase velocity vector (as opposed to the 3D one), obtain maps of TEC disturbances [Huang et al., 2016; Yang et al., 2017; Lay et al., 2018] and all-sky camera images [Shiokawa et al.., 2003, 2009; Syrenova et al., 2022]. This method can, therefore, be useful in developing and improving the models of the neutral wind in the upper thermosphere.

STATISTICAL RELATION OF TRAVELING IONOSPHERIC DISTURBANCES WITH NEUTRAL WIND

The work is based on the representative statistics on MSTID 2D phase velocity vectors obtained from coherent radar data in Ekaterinburg (EKB: 56.4° N, 58.5° E) and Magadan (MGW: 60.0° N, 150.7° E). The method of measuring the MSTID 2D phase velocity vector involves analyzing an HF signal scattered by roughnesses of the Earth surface in the opposite direction, and is described in detail in [Oinats et al., 2015, 2016a, b]. Figure 1 shows the layout of the HF radars.

Black lines indicate sounding directions (radar beams); gray and yellow colors are EKB and MGW radars's fields of view respectively. The MGW radar in 2021 worked only in beams 1–6 and 12 (see Figure 1). The region where TIDs are detected is located approximately in the vicinity of the reflection level of the one-hop HF radio wave trajectory, i.e. approximately between 500 and 800 km from the radar. In Figure 1, this region is marked with red circles. For EKB, the center of the region is ~61° N, 63° E; for MGW, ~62° N, 146° E. The time resolution of the radar systems is ~1 min. Note that in 2012 the EKB radar started to work only in mid-December; and in 2020, it did not work for most of the year due to technical problems.
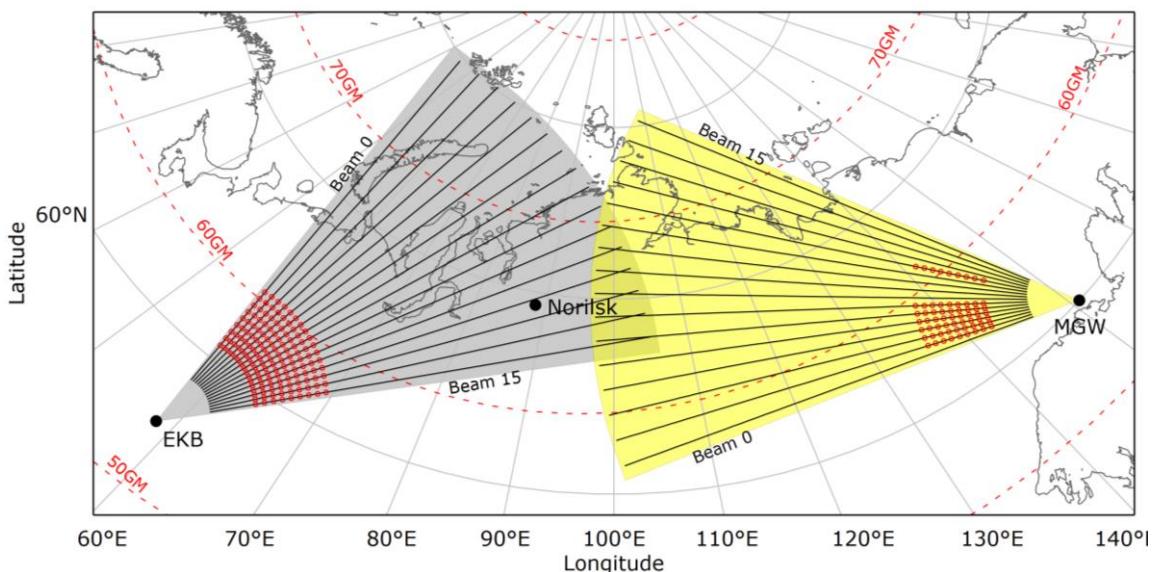

Figure 1. Layout of EKB and MGW HF radars and their fields of view

If the main sources of MSTIDs are IGWs, the temporal dynamics of MSTID azimuths during the day should be determined by the neutral wind. When IGWs propagate downwind, their amplitude decreases greatly due to dissipation, whereas during propagation upwind their amplitude increases [Pogoreltsev, Pertsev, 1996; Waldock, Jones, 1984, 1986]. Thus, the probability of observation increases for the MSTIDs propagating in the direction opposite to the neutral wind at the observation height. On the contrary, in the direction coinciding with a strong neutral wind, the probability of observing MSTIDs is significantly reduced. Thus, maxima in the time distribution of MSTID azimuths should coincide with the directions opposite to the azimuths of the strongest winds that are most frequent in this season and this time of day.

Figure 2 illustrates the distributions of MSTIDs by azimuths, calculated from the geographical north clockwise, and by local time as derived from EKB radar data for different seasons in 2012–2021. Isolines of the neutral wind velocity projection on a given azimuthal direction at a given time are superimposed on the distributions. The wind velocities are calculated by the HWM14 model for the point with coordinates 61° N, 63° E (the center of the TID detection region).

The relative frequency is the ratio of the number of MSTIDs observed in these time and azimuth windows to the total number of MSTIDs observed in this time window. When calculating the distributions, we used windows ±5° in azimuth and ±1 hr in time; the azimuth step was 1°, and the time step was 15 min. The neutral wind velocity was determined from the HWM14 model as a weighted average value according to MSTID distributions (the velocities were averaged with a weight corresponding to the relative frequency of MSTID observation at a given height at a given time). For each MSTID event, we estimated the height at which the measurement was carried out using the model of path characteristics of the HF signal, scattered by the Earth surface, for the EKB radar [Oinats et al., 2016b]. At the MSTID observation height, the meridional and zonal neutral wind velocity components were calculated by the HWM14 model. Then, the resulting array of wind components was subdivided by seasons, and for each season the average value of the components for each local time was computed according to the formula

$$\bar{U}(LT) = \frac{\sum U_i}{N}, \quad \bar{V}(LT) = \frac{\sum V_i}{N}, \qquad (1)$$

where N is the total number of MSTIDs detected over a given period of local time; U_i, V_i are zonal and meridional wind velocity components respectively. Summation is carried out over all values that fall into a given season and a given period of local time. The obtained values were used to calculate the neutral wind projection on each azimuthal direction. Figure 2 indicates that most disturbances (~64 %) are in the region of negative neutral wind projections, as expected. However, in all seasons at ~2–8 hr (with ~240° azimuths in winter, ~210° in spring, ~180° in summer, and ~ 210° in fall), there is

a local maximum of relative frequency in the region of the positive neutral wind velocity projection. In addition, there are local maxima in the region of the positive neutral wind velocity projection: ~16–20 hr with ~0° azimuths in winter, ~16–20 hr with ~210 azimuths in summer, and ~18–22 hr with ~120° azimuths in fall. The reason for this may be both the MSTIDs unrelated to IGWs (for example, various instabilities [Perevalova, Oinats, 2020; Ivanov, Tolstikov, 2003]) and the wind behavior patterns in this region that are not described by the model. Try to determine what we are dealing with in this case. Calculate for each time and azimuth the average horizontal phase velocity of MSTIDs. The velocity of disturbances of any physical nature will increase when propagating downwind and decrease when propagating upwind. Hence, maxima of the MSTID average horizontal velocity correspond to MSTID propagation downwind; and minima, upwind. Thus, if the controversial local maxima correspond to the maxima of the MSTID average horizontal velocity, we can argue that these MSTIDs propagate downwind and, therefore, in this case we are dealing with the MSTIDs that are not manifestations of IGWs. If these local maxima correspond to the minima of the MSTID average horizontal velocity, we can claim that these MSTIDs propagate upwind and hence in this case we are dealing with a wind behavior pattern that is not described by the HWM14 model. Moreover, if the main sources of MSTIDs are IGWs, all local ones should correspond to the minima in the MSTID average horizontal velocity.

Figure 3 illustrates azimuth and local time distributions of the MSTID average horizontal velocity according to EKB radar data. For each azimuth and local time, averaging has been performed over all days of the season and over all years of observations. The isolines corresponding to the relative frequency of MSTID observation are superimposed on the distributions (color part of Figure 2).

Firstly, the local maxima are seen to correspond closely to the minima of the MSTID average horizontal velocity, and we can therefore assert that the main sources of MSTIDs are IGWs. Secondly, the controversial local maxima (~2–8 hr with ~240° azimuths and ~16–20 hr with ~0° azimuths in winter; ~2–8 hr with ~210° azimuths in spring; ~2–8 hr with ~180° azimuths and ~16–20 hr with ~210° azimuths in summer; ~2–8 hr with ~210° azimuths and ~18–22 h with ~120° azimuths in fall) lying, according to HWM14, in the region of the positive neutral wind projection are also in line with the minimum average horizontal velocity of MSTIDs. Thus, we can argue that these MSTIDs propagate upwind, and in this case we are quite likely dealing with the wind behavior pattern that is ignored by HWM14.

The MGW radar data was processed using the same method as for the EKB radar data. Wind velocities were calculated by the HWM14 model for a point with coordinates 62° N, 146° E (center of the MSTID detection region). The processing results are shown in Figures 4, 5.
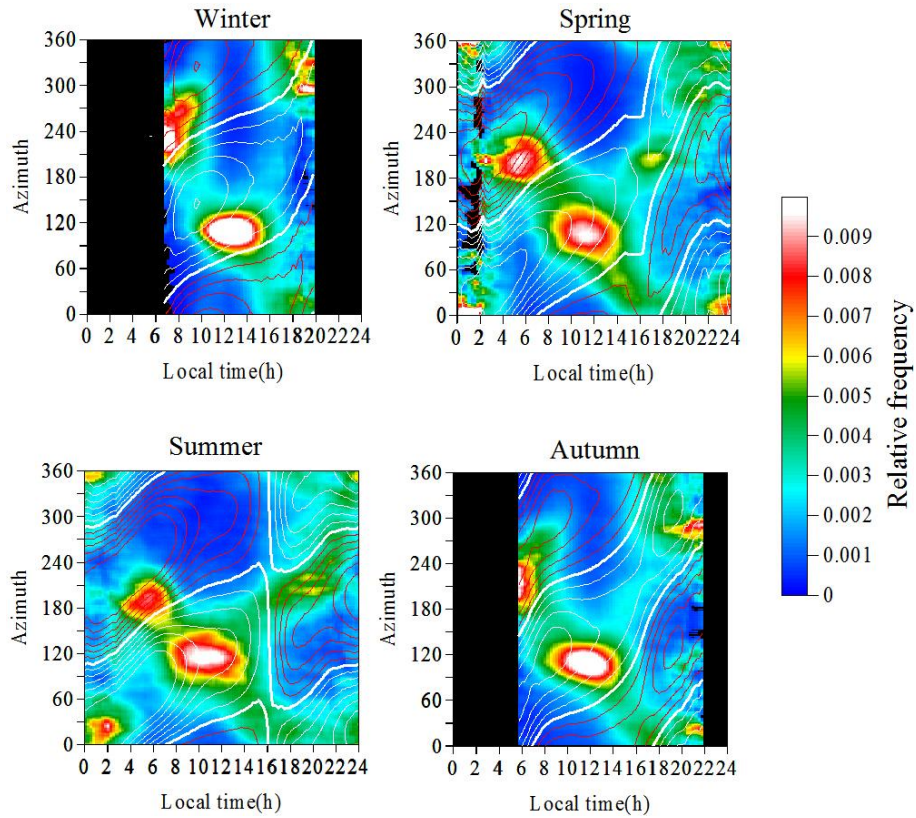
Figure 2. Distribution of MSTIDs by azimuth and local time as derived from EKB radar data for different seasons of 2012–2021 according to the color scale. White isolines indicate negative projections of the neutral wind velocity to a given azimuthal direction at a given time; the bold white line is a zero projection; red isolines show positive projections; the isoline step is 20 m/s. The wind velocities are calculated by the HWM14 model
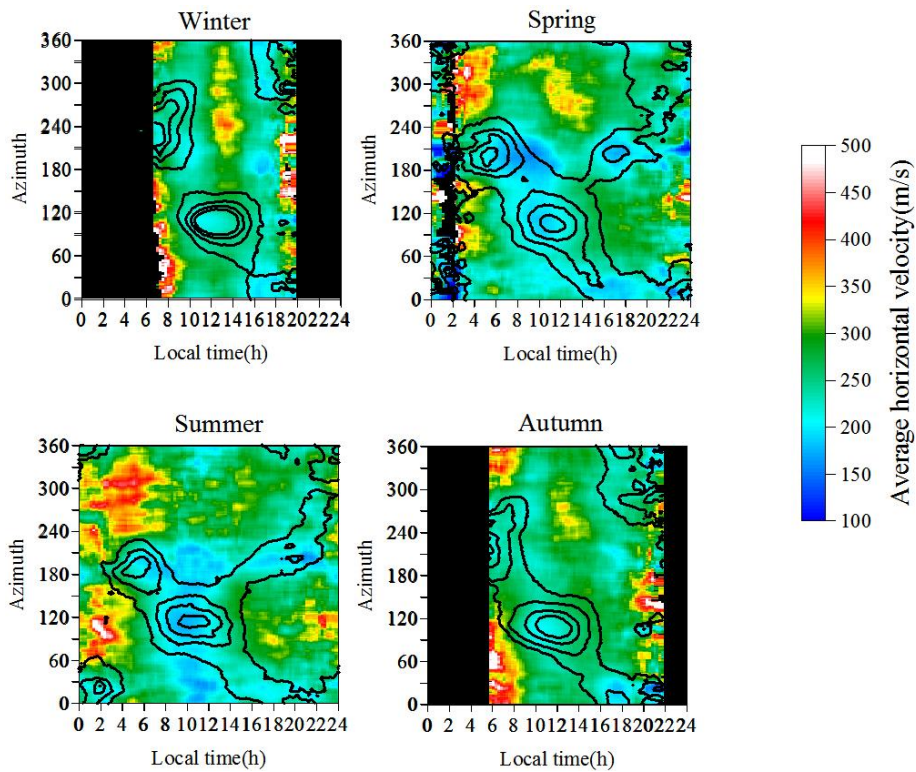

Figure 3. Azimuth and local time distributions of the MSTID average horizontal velocity as observed by the EKB radar. The distributions are superimposed by the isolines corresponding to the relative frequency of MSTID observation. The isolines are drawn at the levels of 0.003, 0.005, 0.007, and 0.009 of the relative frequency of MSTID observation
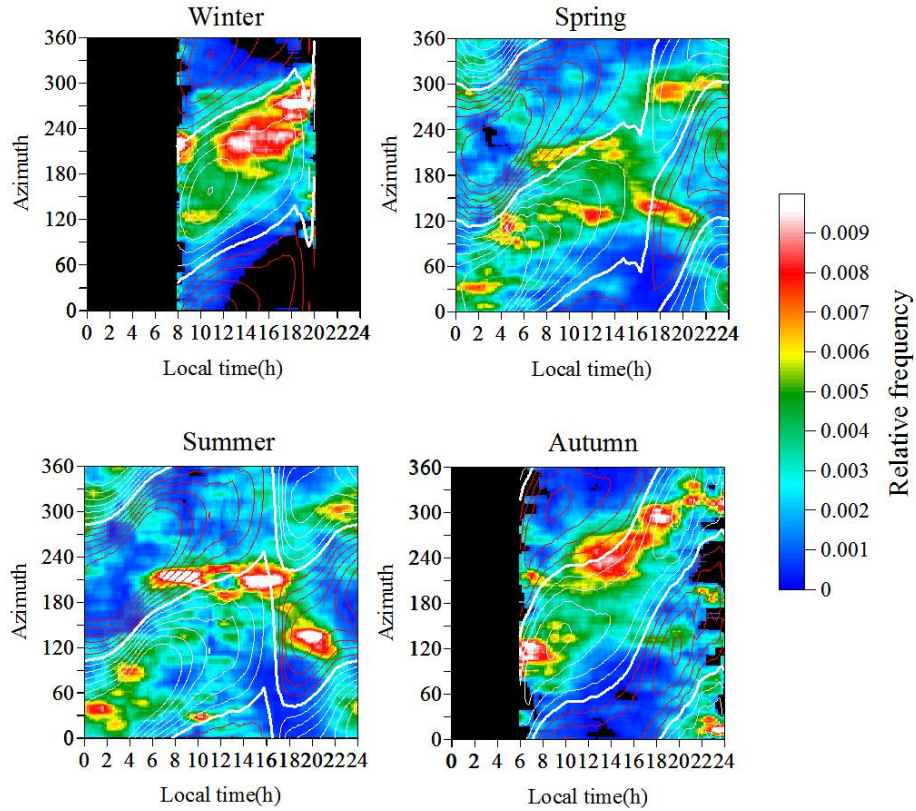
M.V. Tolstikov, A.V. Oinats, M.F. Artamonov, I.V. Medvedeva, K.G. Ratovsky

Figure 4. Azimuth and local time distributions of MSTIDs as derived from MGW radar data for various seasons of 2021 according to the color scale. White isolines indicate negative projections of the neutral wind velocity to a given azimuthal direction at a given time; the bold white line is a zero projection; red isolines show positive projections; the isoline step is 20 m/s. The wind velocities are calculated by the HWM14 model
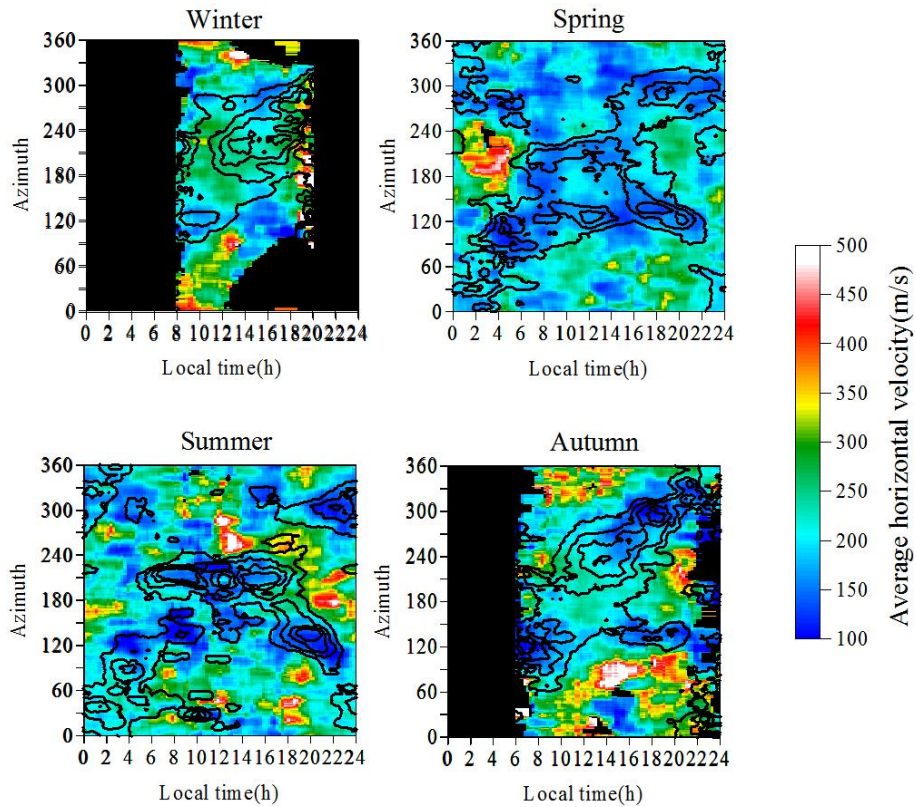
Figure 5. Azimuth and local time distributions of the MSTID average horizontal velocity according to MGW radar data. The distributions are superimposed by the isolines corresponding to the relative frequency of MSTID observation. The isolines are drawn at the levels of 0.003, 0.005, 0.007, and 0.009 of the relative frequency of MSTID observation

Most disturbances are seen to lie in the region of negative neutral wind projections, but there are seasonal peculiarities. In winter, more than 82 % of the disturbances are in the region of negative neutral wind projections; in spring, ~ 56 %; in summer, ~ 55 %; in fall, ~71 %. In the region of positive neutral wind projection, according to HWM14, there are the following controversial local maxima: ~0–4 hr with ~270° azimuths and ~16–20 hr with ~120° azimuths in spring; ~4–8 hr with ~210° azimuths and ~16–21 hr with ~120° azimuths in summer; ~6–8 hr with ~210° azimuths and ~22–24 hr with ~180° azimuths in fall. Let us use the information about the horizontal velocity of MSTIDs to understand whether we are dealing in this case with the MSTIDs unrelated to IGWs or with the wind behavior patterns ignored by HWM14.

The local maxima, including controversial ones (~0–4 hr with ~270° azimuths and ~16–20 hr with ~120° azimuths in spring; ~4–8 hr with ~210° azimuths and ~16–21 hr with ~120° azimuths in summer; ~6–8 hr with ~210° azimuths and ~22–24 hr with ~180° azimuths in fall), are seen to correspond closely to the minimum average horizontal velocity of MSTIDs. We can, therefore, assert that, firstly, the main sources of MSTIDs are IGWs, and secondly, the controversial maxima are probably explained by the wind behavior pattern ignored by HWM14.

Thus, we can conclude that distributions of the MSTID parameters contain information on the neutral wind. Let us check this with another example. During major sudden stratospheric warmings (SSWs), significant variations in the neutral wind can be expected. Since the SSW effect is ignored in the HWM14 model, we can assume that during SSWs the greatest difference between the model and reality will be observed, i.e. most MSTIDs lying in the region of the positive wind projection identified by HWM14.

STATISTICAL RELATION OF TRAVELING IONOSPHERIC DISTURBANCES WITH SUDDEN STRATOSPHERIC WARMINGS

According to the definition offered by the World Meteorological Organization, SSW can be classified as major when in winter the average zonal wind at a latitude of 60° N and an altitude level of 10 hPa (~32 km) changes its direction from west to east and the zonal temperature gradient of the stratosphere at 10 hPa between 60° N and 90° N becomes positive [Labitzke, Naujokat, 2000]. Tolstikov et al. [2019] have examined the influence of major SSWs on MSTIDs in the ionosphere, using Hokkaido radar data, and have shown that during such events the anisotropy of the MSTID observation frequency changes significantly with propagation direction. Namely, before warming there is a characteristic distribution of MSTID azimuths with a pronounced maximum at ~120° (note that this is a typical distribution for the winter season in Hokkaido); during warming, additional maxima appear; and after warming, the distribution returns to its original shape.

Consider the effect of major SSWs on the disturbance in the ionosphere according to the EKB radar data. Figure 6 illustrates MSTID distributions by days of the year and azimuths: averaged over 2012–2021 and for 2013, when a major SSW event occurred in January.

The relative frequency was calculated in the same way as in the previous cases, but we used a window ±5° in azimuth and ±5 days in days of the year; the azimuth step is 1°; step in days of the year, one day. Variations in the zonal mean neutral wind velocity over the Northern Hemisphere were analyzed using MERRA reanalysis data (Modern ERA-Ret-prospective Analysis for Research and Applications) [Gelaro et al., 2017]. Vertical red lines indicate reversal of the atmospheric zonal circulation at 60° N, 10 hPa. It is evident that in winter the prevailing direction of MSTID propagation has an azimuth of ~110°. Note that the radar operates at a constant frequency of ~11 MHz. At night in winter, the electron density of the ionospheric F2-region at midlatitudes becomes so low that the HF signal of this frequency is not reflected from the ionosphere. That is why at night in winter, MSTID parameters cannot be measured with the HF radar [Oinats et al., 2015, 2016a], and the ~110° azimuth, seen in Figure 6, corresponds to the dominant direction of propagation of disturbances in the daytime. Comparing the left and right panels shows that during warming the azimuth distribution "breaks down",
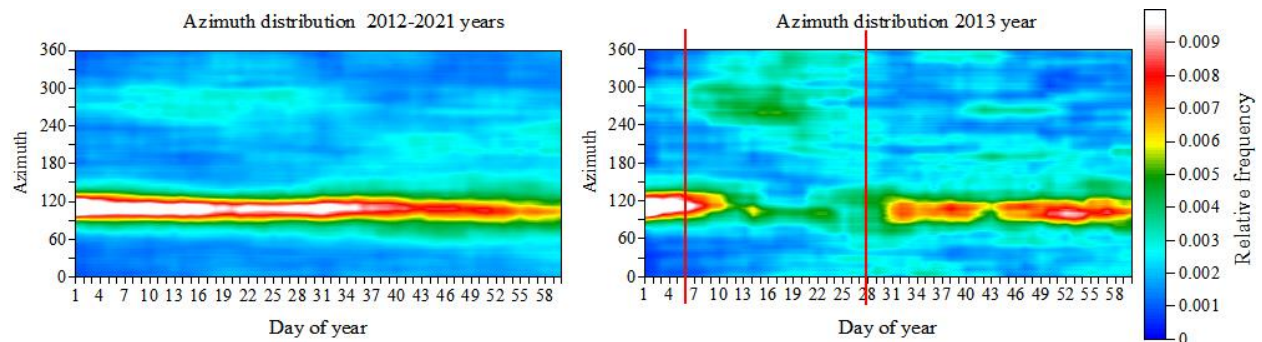

Figure 6. Distributions of the relative frequency of MSTID observations with the EKB HF radar by days of the year and azimuths: averaged over 2012–2021 (left) and for 2013 (right). Vertical red lines mark the dates when the zonal stratospheric circulation changed direction at 60° N, 10 hPa

additional local maxima appear, and after warming the distribution returns to its original shape. A similar effect was also observed by the Hokkaido HF radar [Tolstikov et al., 2019].

Following [Tolstikov et al., 2019], we estimate the perturbation of the azimuth distribution of MSTIDs and the perturbation of the zonal circulation velocity. Determine the annual average variations in zonal circulation over a long period of time and consider the absolute value of the difference between variations for a particular year and mean variations as perturbations of annual variations. Figure 7 depicts the zonal mean neutral wind velocity at 60° N and 10 hPa according to the MERRA reanalysis. The thick red line is the average velocity calculated for the period from 2003 to 2021; colored lines are velocities for individual years. It is clearly seen that the zonal mean velocity variations can differ significantly from year to year, especially in fall, winter, and spring.

Similarly, we calculate the variations in the azimuth distributions of MSTIDs. Determine the annual average azimuth distributions of MSTIDs *AvDist* for each day and calculate the perturbation of the azimuth distribution of MSTIDs for the *i*-th day of the *j*-th year by the formula

$$AzmVar = \sqrt{\frac{1}{360} \sum_{\phi}^{359} \left(Dist(i, j, \phi) - AvDist(i, \phi) \right)^2}. \quad (2)$$

Here $Dist(i, j, \phi)$ is the relative frequency of MSTIDs with azimuth for the *i*-th day of the *j*-th year; $AvDist(i, \phi)$ is the average relative frequency for azimuth ϕ for the *i*-th day. Figure 8 shows, for comparison, the zonal mean wind disturbances for the SSW period of 2013 and the disturbance in MSTID azimuth distributions calculated from Formula (2).

The zonal mean wind disturbances are seen to correlate well with the disturbance of the MSTID azimuth distribution (~0.825 correlation coefficient), which allows us to assert that disturbances in the lower atmosphere have an effect on ionospheric disturbances. Tolstikov et al. [2019] have proposed the following mechanism of this effect: planetary waves (not neces-

sarily those associated with the reversal of the polar vortex) cause changes in the neutral wind in the mesopause region, which leads to a change in the IGW propagation directions restricted by the neutral wind. Since the HWM14 model ignores SSWs, the greatest differences between the model and observations can be expected during these events. Figure 9 shows zonal mean wind disturbances (red line) and the percentage of MSTIDs propagating in the neutral wind, as derived from the HWM14 model (green line).

It can be seen that during the SSW period in 2013 the largest number of "incorrect" MSTIDs, i.e. lying in the region of positive neutral wind projections, did occur. The correlation coefficient of the curves is ~0.85.

METHOD FOR ESTIMATING THE NEUTRAL WIND FROM DISTRIBUTIONS OF MSTID PARAMETERS

We have shown above that the distributions of MSTID parameters contain information about the neutral wind. Tolstikov et al. [2020] have proposed a method for estimating the neutral wind azimuth from the distribution of the relative frequency of MSTID azimuth observation. The method involves finding the maximum of the optimized function depending on the azimuth of the horizontal neutral wind. For each instant of time, all possible directions are searched (0°–359°), and it is calculated how many MSTIDs are in the region of the negative neutral wind projection, and how many are in the region of the positive neutral wind projection. The optimized function looks as follows:

$$I(\alpha) = -\sum_{\phi=0}^{\phi=359} N(t, \phi) \cos(\overset{\wedge}{\alpha}\phi) \to \max, \quad (3)$$

where $N(t, \phi)$ is the relative frequency of observations of MSTIDs propagating at *t* with ϕ, and $\overset{\wedge}{\alpha}\phi$ is the angle
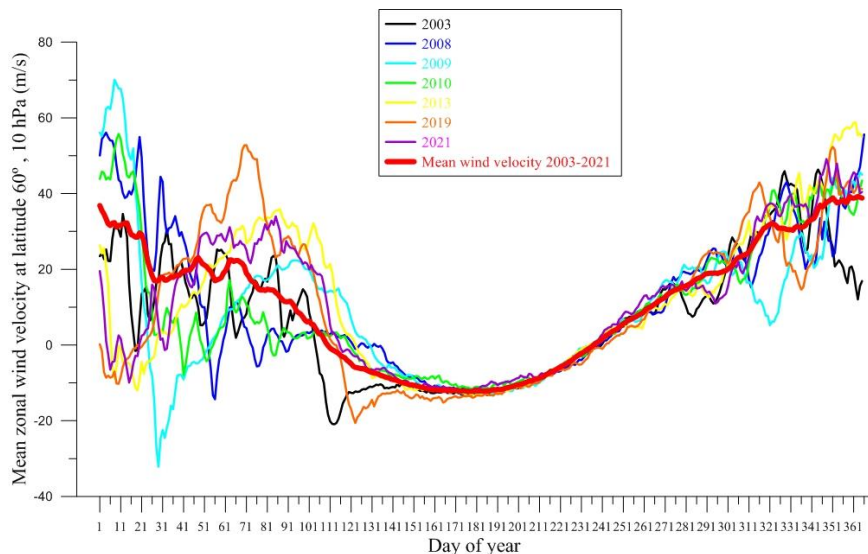
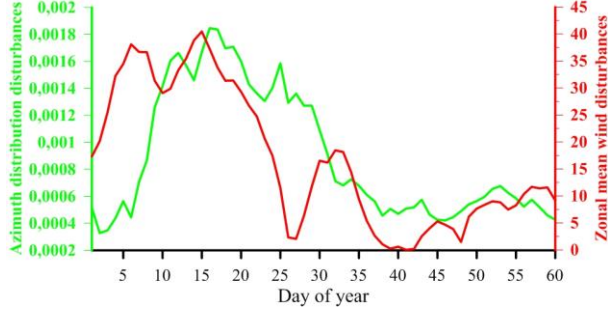*Figure 7.* Zonal mean wind velocity variations at 60° N and 10 hPa

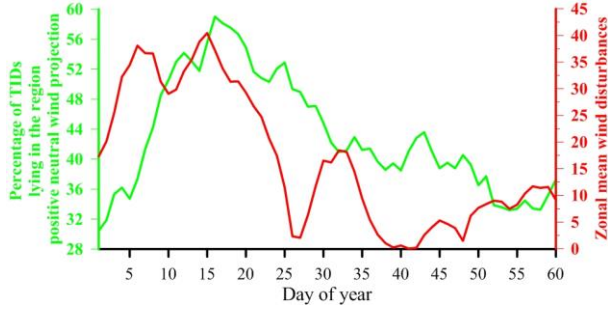*Figure 8*. Wind disturbances (red line) versus MSTID azimuth disturbances (green line)

Figure 9. Zonal mean wind disturbances (red line) versus the number of TIDs (in percent) lying in the region of the positive neutral wind projection according to the HWM14 model (green line)

between the MSTID propagation direction and the wind velocity. The angle α, which provides the maximum of the function *I*, is taken for the neutral wind azimuth. A question arises as to whether it is possible to determine the zonal and meridional neutral wind velocities by measuring the two-dimensional phase velocity vector of MSTIDs assuming that they are a manifestation of IGWs. When the IGW full velocity vector is measured, the dispersion equation for IGWs can be used to determine the internal frequency, and then the wind velocity projection on the IGW propagation direction:

$$U_{\mathrm{p}} = (f - f')L_{\mathrm{H}}. \qquad (4)$$

Here L_{H} is the IGW horizontal wavelength. With representative observation statistics available, we can find zonal U_x and meridional U_y wind velocities from the functional

$$\sum (U_x \sin\phi + U_y \cos\phi - U_p)^2 \to \min. \qquad (5)$$

This method is described in detail in [Medvedev et al., 2015, 2017]. If the neutral wind azimuth is known (for example, from (3)), the Boussinesq dispersion equation [Pedlosky, 2003] can yield the expression

$$\sum \left(L_{\mathrm{H}_i} - \frac{U\cos(\alpha_i) + L_i f_{\mathrm{B}}}{f_i} \right)^2 \to \min. \qquad (6)$$

Here L is the total wavelength of IGW; U is the wind velocity modulus; f is the IGW frequency; f_{B} is the Brent frequency; α is the angle between neutral wind directions and IGW propagation direction. If the IGW 2D phase velocity vector is measured, we know all parameters included in (6), except for the IGW full wavelength.

Automatic methods of processing simultaneous measurement data from the Irkutsk Incoherent Scatter Radar and the Irkutsk ionosonde DPS-4 provided representative statistics on 3D parameters of TID propagation in the ionosphere [Medvedev et al., 2013, 2015]. Given that the statistics on TID parameters at midlatitudes does not depend much on longitude, we can use the median wavelength from the Irkutsk data. For winter, spring, and fall, the median wavelength is ~260 km; for summer, ~300 km. By determining the neutral wind azimuth from (3) and the velocity modulus from (6), we can obtain the zonal and meridional neutral wind velocities. Since very significant assumptions were used, this method can only be called an estimate of the neutral wind, rather than a measurement. Nevertheless, it can be very useful because there are few ways to perform round-the-clock measurement of the neutral wind in the thermosphere. Figure 10 presents the results of estimation of zonal (left) and meridional (right) neutral wind velocities as a function of local time for four seasons according to EKB observations of MSTIDs (green line). For comparison, the calculations performed using the HWM14 model (red line) for the MSTID observation height are given.

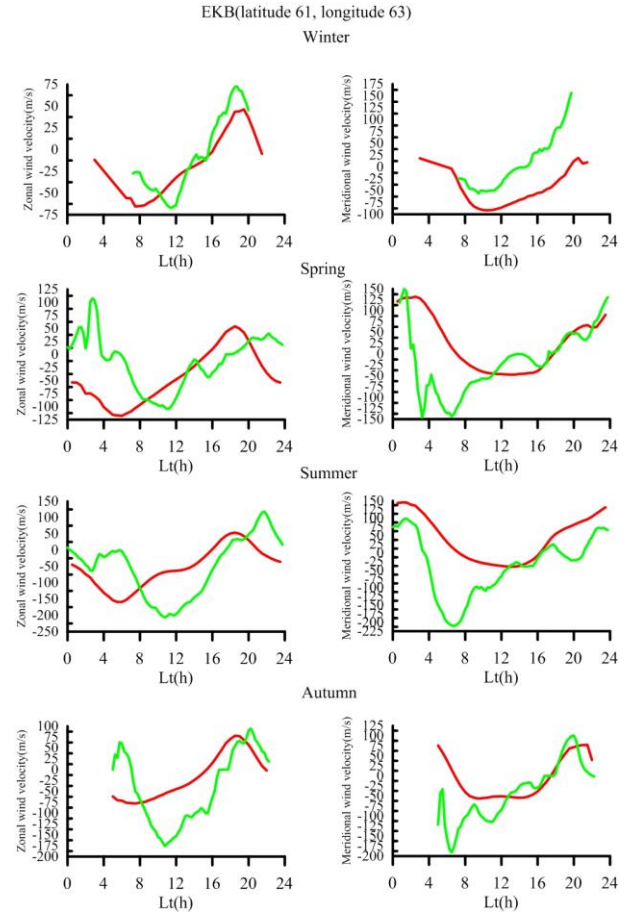Figure 11 presents similar results from the MGW radar data.

Figure 10. Calculations of zonal (left) and meridional (right) neutral wind velocity components for the EKB radar: red line — HWM14, green line — calculations
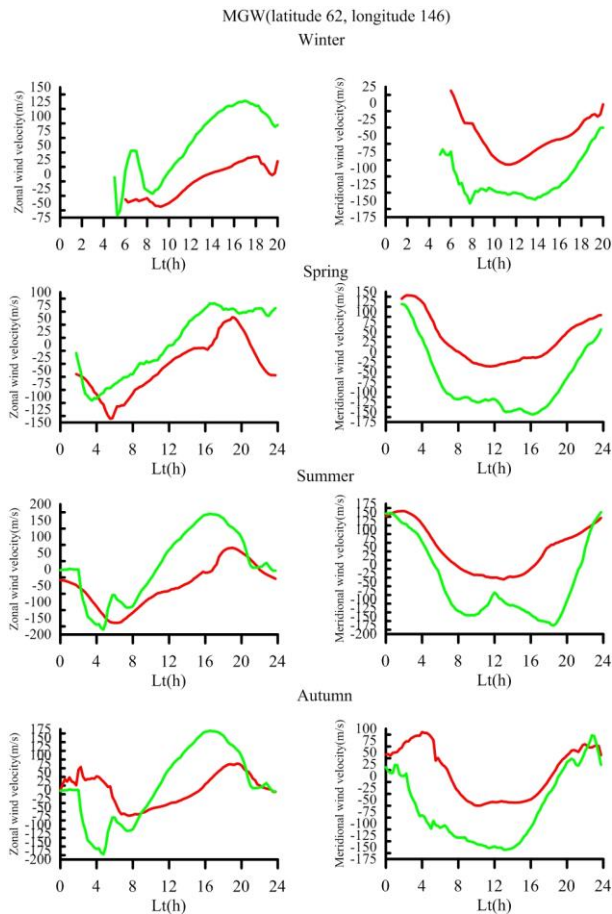
MGW(latitude 62, longitude 146)
Winter
Spring
Summer
Autumn

Figure 11. The same as in Figure 10 for the MGW radar

It can be seen from Figures 10, 11 that the neutral wind parameters are in satisfactory agreement with the HWM14 data. The difference with the models can be explained by traveling ionospheric disturbances unrelated to IGWs, or by the wind features ignored by HWM. The proposed method is universal and makes it possible to estimate the zonal and meridional neutral wind velocities from the statistics on observations of the 2D phase velocity vector of IGWs obtained by any instrument.

CONCLUSIONS

Analysis of the statistical relation of traveling ionospheric disturbances with the neutral wind and stratospheric disturbances has yielded the following results.

Comparison of the azimuth and local time distributions of the relative frequency of MSTID observations and MSTID average velocities with the distributions of wind velocities at the heights of observations of MSTIDs, calculated using the HWM14 model, has revealed that most MSTIDs fit the wind-filtering hypothesis. Thus, we can argue that the main sources of MSTIDs are IGWs from the underlying atmosphere with a possible contribution of IGWs from the middle atmosphere, which have not been filtered by the underlying atmosphere.

During major stratospheric disturbances, the azimuthal distribution of MSTIDs changes significantly. The deviation from the average distribution correlates well with the disturbances of the zonal mean wind velocity at a latitude of 60° and an altitude level of 10 hPa.

The deviation from the average distribution is likely to be related to the change in the neutral wind in the upper thermosphere.

A method for estimating the neutral wind from the statistics on MSTID 2D phase velocity vectors has first been proposed. The method is based on the assumption that the main sources of MSTIDs are IGWs from the underlying atmosphere. The method was tested on the data from the EKB and MGW HF radars. The estimated neutral wind parameters are in satisfactory agreement with HWM14 data, and the differences may be explained by the presence of MSTIDs unrelated to IGWs or by the wind features ignored by the model. Note that since we have used very significant assumptions (the possibility of using the median wavelength and the fact that the statistics on mid-latitude TID parameters does not depend much on longitude), this method can only be called an estimate of the neutral wind, and not a measurement. Nevertheless, this method can be very useful because it can estimate the zonal and meridional neutral wind velocities from measurements of the IGW horizontal phase velocity vector, which are more common than measurements of the full vector. In particular, there are methods for estimating horizontal parameters of MSTID from all-sky camera data and from TEC maps. Thus, the proposed method can be useful in developing and improving neutral wind models.

Comprehensive study into the manifestation of wave activity with IGW periods in various regions of the atmosphere allowed us to assess the influence of wave activity in the stratosphere and planetary waves on wave activity at ionospheric heights.

REFERENCES

Afraimovich E.L., Kosogorov E.A., Leonovich L.A., Palamartchouk K.S., Perevalova N.P., Pirog O.M. Determining parameters of large-scale traveling ionospheric disturbances of auroral origin using GPS-arrays. *J. Atmos. Solar-Terr. Phys.* 2000, vol. 62, iss. 7, pp. 553–565. DOI: 10.1016/S1364-6826(00)00011-0.

Alexander M.J., Gille J., Cavanaugh C., Coffey M., Craig C., Eden T., et al. Global estimates of gravity wave momentum flux from High Resolution Dynamics Limb Sounder observations. *J. Geophys. Res.* 2008, vol. 113, no. D15, pp. 1–11. DOI: 10.1029/2007jd008807.

Crowley G., Jones T.B., Dudeney J.R. Comparison of short period TID morphologies in Antarctica during geomagnetically quiet and active intervals. *J. Atmos. Terr. Phys.* 1987, vol. 49, pp. 1155–1162.

Drob D.P., Emmert J.T., Crowley G., Picone J.M., Shepherd G.G., Skinner W., et al. An empirical model of the Earth's horizontal wind fields: HWM07. *J. Geophys. Res.* 2008, vol. 113, iss. A12, citeID A12304. DOI: 10.1029/2008JA013668.

Drob D.P., Emmert J.T., Meriwether J.W., Makela J.J., Doornbos E., Conde M., et al. An update to the Horizontal Wind Model (HWM): The quiet time thermosphere. *Earth and Space Sci.* 2015, vol. 2, pp. 301–319. DOI: 10.1002/2014EA000089.

Fritts D.C., Alexander M.J. Gravity wave dynamics and effects in the middle atmosphere. *Rev. Geophys.* 2003, vol. 41, pp. 1003–1066. DOI: 10.1029/2001RG000106.

Gelaro R., McCarty W., Suárez M.J., Todling R., Molod A., Takacs L., et al.The Modern-Era Retrospective Analysis for Research and Applications, Version 2 (MERRA-2). *J. Climate.* 2017, vol. 30, no. 14, pp. 5419–5454. DOI: 10.1175/JCLI-D-16-0758.1.

Hines C.O. Internal gravity waves at ionospheric heights. *Can. J. Phys.* 1960, vol. 38, pp. 1441–1481.

Huang F., Dou X., Lei J., Lin J., Ding F., Zhong J. Statistical analysis of nighttime medium-scale traveling ionospheric disturbances using airglow images and GPS observations over central China. *J. Geophys. Res.: Space Phys.* 2016, vol. 121, no. 9, pp. 8887–8899. DOI: 10.1002/2016JA022760.

Ivanov V.B., Tolstikov M.V. Instability of the state of the night-time topside ionosphere. *J. Atmos. Solar-Terr. Phys.* 2003, vol. 65, no. 6, pp. 673–676. DOI: 10.1016/S1364-6826(03)00080-4.

Kalikhman A.D. Medium-scale traveling ionospheric disturbances and thermospheric winds in the F-region. *J. Atmos. Solar-Terr. Phys.* 1980, vol. 42, pp. 697–703.

Labitzke K., Naujokat B. The lower Arctic stratosphere in winter since 1952. *SPARC Newslett.* 2000, vol. 15, pp. 11–14.

Lay E.H., Parker P.A., Light M., Carrano C.S., Debchoudhury S., Haaser R.A. Midlatitude ionospheric irregularity spectral density as determined by ground-based GPS receiver networks. *J. Geophys. Res.: Space Phys.* 2018, vol. 123, no. 6, pp. 5055–5067, DOI: 10.1029/2018JA025364.

Ma S.Y., Schlegel K., Xu J.S. Case studies of the propagation characteristics of auroral TIDs with EISCATCP2 data using maximum entropy cross-spectral analysis. *Ann. Geophys.* 1998, vol. 16, iss. 2, pp. 161–167. DOI: 10.1007/S00585-998-0161-3.

Medvedev A.V., Ratovsky K.G., Tolstikov M.V., Alsatkin S.S., Scherbakov A.A. Studying of the spatial-temporal structure of wavelike ionospheric disturbances on the base of Irkutsk Incoherent Scatter Radar and Digisonde data. *J. Atmos. Solar-Terr. Phys.* 2013, vol. 105–106, pp. 350–357. DOI: 10.1016/j.jastp.2013.09.001.

Medvedev A.V. Ratovsky K.G., Tolstikov M.V., Alsatkin S.S., Scherbakov A.A. A statistical study of internal gravity wave characteristics using the combined Irkutsk Incoherent Scatter Radar and Digisonde data. *J. Atmos. Solar-Terr. Phys.* 2015, vol. 132, pp. 13–21. DOI: 10.1016/j.jastp.2015.06.012.

Medvedev A.V., Ratovsky K.G., Tolstikov M.V., Oinats A.V., Alsatkin S.S., Zherebtsov G.A. Relation of internal gravity wave anisotropy with neutral wind characteristics in the upper atmosphere. *J. Geophys. Res.: Space Phys.* 2017, vol. 122, pp. 7567–7580. DOI: 10.1002/2017JA024103.

Medvedev A.V., Ratovsky K.G., Tolstikov M.V., Vasilyev R.V., Artamonov M.V. Method for determining neutral wind velocity vectors using measurements of internal gravity wave group and phase velocities. *Atmosphere.* 2019, vol. 10, no. 9, p. 546. DOI: 10.3390/atmos10090546.

Negale M.R., Taylor M.J., Nicolls M.J., Vadas S.L., Nielsen K., Heinselman C.J. Seasonal propagation characteristics of MSTIDs observed at high latitudes over Central Alaska using the Poker Flat Incoherent Scatter Radar. *J. Geophys. Res.: Space Phys.* 2018, vol. 123, pp. 5717–5737. DOI: 10.1029/ 2017JA024876.

Nicolls M.J., Heinselman C.J. Three-dimensional measurements of traveling ionospheric disturbances with the Poker Flat Incoherent Scatter Radar. *Geophys. Res. Lett.* 2007, vol. 34, p. L21104. DOI: 10.1029/2007GL031506.

Nicolls M.J., Vadas S.L., Aponte N., Sulzer M.P. Horizontal parameters of daytime thermospheric gravity waves and E region neutral winds over Puerto Rico. *J. Geophys. Res.: Space Phys.* 2014, vol. 119, pp. 575–600, DOI: 10.1002/2013JA018988.

Oinats A.V., Kurkin V.I., Nishitani N. Statistical study of medium-scale traveling ionospheric disturbances using SuperDARN Hokkaido ground backscatter data for 2011. *Earth, Planets and Space.* 2015, article id. 22, 9 p. DOI: 10.1186/s40623-015-0192-4.

Oinats A.V., Nishitani N., Ponomarenko P., Berngardt O., Ratovsky K.G. Statistical characteristics of medium-scale traveling ionospheric disturbances revealed from the Hokkaido East and Ekaterinburg HF radar data. *Earth, Planets and Space.* 2016a, vol. 68, no. 8. DOI: 10.1186/s40623-016-0390-8.

Oinats A.V., Nishitani N., Ponomarenko P., Ratovsky K.G. Diurnal and seasonal behavior of the Hokkaido East ground backscatter: simulation and observation. *Earth, Planets and Space.* 2016b, vol. 68, article id. 18, 12 p. DOI: 10.1186/s40623-015-0378-9.

Otsuka Y. Medium-Scale Traveling Ionospheric Disturbances. *Geophys. Monograph Ser. Ionosphere Dynamics and Applications.* 2021. pp. 421–437. DOI: 10.1002/9781119815617.ch18.

Pedlosky J. *Waves in the Ocean and Atmosphere: Introduction to Wave Dynamics.* Springer, 2003, USA, 260 p.

Perevalova N.P., Oinats A.V. *Morphology of nighttime medium-scale traveling ionospheric disturbances in the midlatitude F region (Review of Modern Concepts).* Irkutsk, ISU Publ. 2020, 83 p. (In Russian).

Pogoreltsev A.I., Pertsev N.N. The influence of background wind on the formation of the acoustic-gravity wave structure in the thermosphere. *Izvestiya. Atmospheric and Oceanic Phys.* 1996, vol. 132, no. 6, pp. 723–728.

Shcherbakov A.A., Medvedev A.V., Kushnarev D.S., Tolstikov M.V., Alsatkin S.S. Calculation of meridional neutral winds in the middle latitudes from the Irkutsk Incoherent Scatter Radar. *J. Geophys. Res.: Space Phys.* 2015, vol. 120, pp. 10851–10863. DOI: 10.1002/2015JA021678.

Shiokawa K., Ihara C., Otsuka Y., Ogawa T. Statistical study of nighttime medium-scale traveling ionospheric disturbances using midlatitude airglow images. *J. Geophys. Res.* 2003, vol. 108, iss. A1, CiteID 1052. DOI: 10.1029/2002JA009491.

Shiokawa K., Otsuka Y., Ogawa T. Propagation characteristics of nighttime mesospheric and thermospheric waves observed by optical mesosphere thermosphere imagers at middle and low latitudes. *Earth, Planets and Space.* 2009, vol. 61, pp. 479–491. DOI: 10.1186/BF03353165.

Syrenova T.E., Beletsky A.B., Ratovsky K.G., Tolstikov M.V., Vasilyev R.V. Morphology of traveling wave disturbances recorded in Eastern Siberia in 630 nm atomic oxygen emission. *Atmosphere.* 2022, vol. 13, iss. 2, p. 198. DOI: 10.3390/ atmos13020198.

Tolstikov M.V., Oinats A.V., Medvedeva I.V., Medvedev A.V., Ratovsky K.G., Nishitani N. Relation of traveling ionospheric disturbances characteristics with planetary waves in the middle atmosphere. *Proc. PhotonIcs & Electromagnetics Research Symposium*, 2019. Spring (PIERS-Spring), Rome, Italy, 2019, pp. 2176–2182. DOI: 10.1109/PIERS-Spring46901.2019.9017884.

Tolstikov M.V., Oinats A.V., Medvedeva I.V., Nishitani N. Method for estimating neutral wind azimuth using 2D TID propagation parameters. *Proc. 2020 XXXIIIrd General Assembly and Scientific Symposium of the International Union of Radio Science.* Rome, Italy, 2020. P. 1–4. DOI: 10.23919/URSIGASS49373.2020.9232189.

Vadas S.L., Nicolls M.J. Using PFISR measurements and gravity wave dissipative theory to determine the neutral background thermospheric winds. *Geophys. Res. Lett.* 2008, vol. 35, iss. 2. CiteID L02105. DOI: 10.1029/2007GL031522.

Van de Kamp M., Pokhotelov D., Kauristie K. TID characterized using joint effort of incoherent scatter radar and GPS. *Ann. Geophys.* 2014, vol. 32, pp. 1511–1532. DOI: 10.5194/angeo-32-1511-2014.

Vlasov A., Kauristie K., Van de Kamp M., Luntama J.-P., Pogoreltsev A. A study of traveling ionospheric disturbances and atmospheric gravity waves using EISCAT Svalbard Radar IPY-data. *Ann. Geophys.* 2011, vol. 29, pp. 2101–2116. DOI: 10.5194/angeo-29-2101-2011.

Waldock J.A., Jones T.B. The effects of neutral winds on the propagation of medium-scale atmospheric gravity waves at mid-latitudes. *J. Atmos. Terr. Phys.* 1984, vol. 46, pp. 217–231. DOI: 10.1016/0021-9169(84)90149-1.

Waldock J.A., Jones T.B. HF Doppler observations of medium-scale travelling ionospheric disturbances at mid-latitudes. *J. Atmos. Terr. Phys.* 1986, vol. 48, pp. 245–260. DOI: 10.1016/0021-9169(84)90149-1.

Williams P.J.S., Van Eyken A.P., Bertin F. A test of the Hines dispersion equation for atmospheric gravity waves. *J. Atmos. Solar-Terr. Phys.* 1982, vol. 44, no. 7, pp. 573–576. DOI: 10.1016/0021-9169(82)90067-8.

Yang H., Monte-Moreno E., Hernández-Pajares M., Multi-TID detection and characterization in a dense global navigation satellite system receiver network. *J. Geophys. Res.: Space Phys.* 2017, vol. 122, no. 9, pp. 9554–9575. DOI: 10.1002/2017JA023988.

URL: http://ckp-rf.ru/ckp/3056 (accessed July 28, 2022).
URL: http://ckp-rf.ru/usu/77733 (accessed July 28, 2022).

How to cite this article
Tolstikov M.V., Oinats A.V., Artamonov M.F., Medvedeva I.V., Ratovsky K.G. Statistical relation of traveling ionospheric disturbances with neutral wind and disturbances in the stratosphere. *Solar-Terrestrial Physics.* 2022. Vol. 8. Iss. 4. P. 78–88. DOI: 10.12737/stp-84202208.